iScience

CellPress
OPEN ACCESS

Article

The RBPMS$^{CreERT2\text{-}tdTomato}$ mouse line for studying retinal and vascular relevant diseases

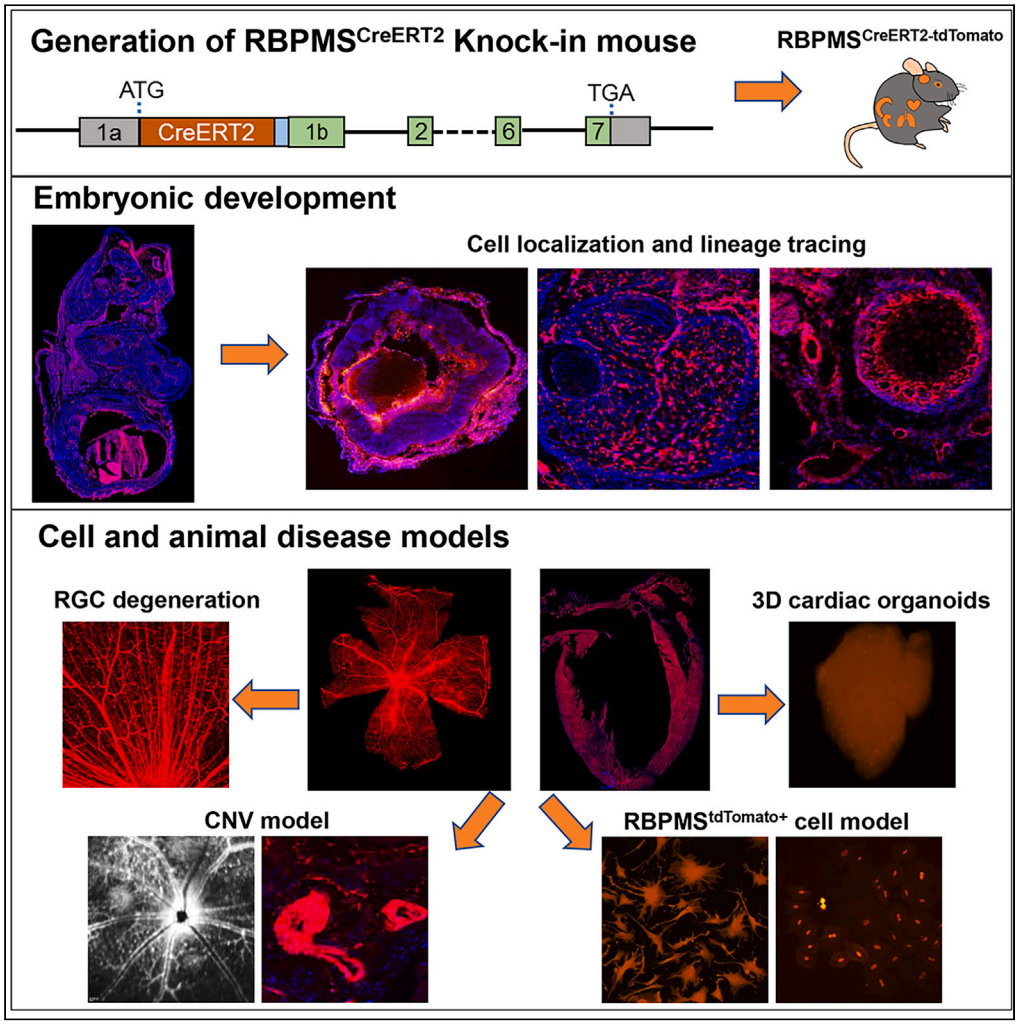

Guilan Li, Yuanting Luo, Qikai Zhang, Wenfei Chen, Kunbei Lai, Yizhi Liu, Yingfeng Zheng

zhyfeng@mail.sysu.edu.cn

Highlights

Generation of RBPMS$^{CreERT2\text{-}tdTomato}$ reporter mouse line

This model can be used for RBPMS^{+} cells linage tracing across various tissues

Exploring the mechanisms of RGCs degeneration and choroidal neovascularization

RBPMS-tdTomato in SMCs and pericytes can be used for non-invasive vascular examination

Li et al., iScience 26, 108111
November 17, 2023
https://doi.org/10.1016/j.isci.2023.108111

iScience

CellPress
OPEN ACCESS

Article

The RBPMS$^{CreERT2\text{-}tdTomato}$ mouse line for studying retinal and vascular relevant diseases

Guilan Li,[1,2] Yuanting Luo,[1] Qikai Zhang,[1] Wenfei Chen,[1] Kunbei Lai,[1] Yizhi Liu,[1,2] and Yingfeng Zheng[1,2,3,*]

SUMMARY

RNA-binding protein with multiple splicing (RBPMS) plays a crucial role in cardiac mesoderm specification and cardiovascular development, as well as being a typical marker for whole retinal ganglion cells (RGCs). However, there is a lack of animal models to spatiotemporally trace the location and function of RBPMS-expressing cells *in vivo*. In this study, we develop a tamoxifen-inducible RBPMS-tdTomato reporter mouse line to track RBPMS-expressing cells during embryogenesis and adulthood. This mouse line allows us to identify and locate RBPMS-tdTomato-positive cells among various tissues, especially in RGCs and smooth muscle cells, which assist to simulate related retinal degenerative diseases, model and examine choroidal neovascularization non-invasively *in vivo*. Our results show that the RBPMS$^{CreERT2\text{-}tdTomato}$ mouse line is a valuable tool for lineage tracing, disease modeling, drug screening, as well as isolating specific target cells.

INTRODUCTION

RBPMS (RNA-binding protein with multiple splicing), also known as Hermes, is a member of the RNA recognition motif family of RNA-binding proteins. These genes typically contain conserved RNA-binding motifs which play a crucial role in posttranscriptional gene expression regulation.[1,2] Previous research has shown that RBPMS is expressed in various organs such as the heart, muscle, vascular system, lung, kidney, liver, and eye.[3] However, most studies on RBPMS have focused on its role in the development and function of cardiomyocytes and vascular smooth cells, specifically in mediating cardiomyocyte binucleation and the maturity of vascular smooth cells.[4,5] Additionally, RBPMS has been identified as a typical marker of retinal ganglion cells (RGCs); however, there is currently a lack of definitive evidence for its functional role in RGCs.[6,7]

RGCs are specialized neurons that play a crucial role in the visual system by receiving and transmitting signals from the retina to the brain through their optic nerve axons. RGCs are particularly vulnerable to a variety of sight-threatening diseases such as glaucoma, diabetic retinopathy, optic neuritis, and optic nerve crush, which can result in the loss of RGCs and lead to blindness.[8] To gain a better understanding of the characteristics of RGCs and the underlying pathological mechanisms, researchers have developed various RGC-reporter knockin (KI) mice models, such as Thy1 mice[9,10] and Brn3/Pou4F mice.[11–14] Thy1 is a cell surface glycoprotein that was first discovered in mature T lymphocytes in mice.[15] It has also been found to be expressed in the central nervous system[16] and RGCs.[17] Transgenic mice lines expressing XFP (YFP, CFP, GFP, and RFP) under the Thy1 promoter have shown that labeled cells are either not specific or only a subset of RGCs, with variable fluorescence intensity of somata and axons, even between lines.[18] Brn3/Pou4F plays an important role in RGC development and type specification, and established reporter knockin mice can be used for precise identification of RGCs, but they only represent a part of RGCs. One previous study showed that nearly 96% RBPMS^{+} RGC cells were co-expressing with vesicular glutamate transporter 2 (VGLUT2)-tdTomato, which speculated that VGLUT2 might be a marker of RGC. However, they also showed small fraction of cones photoreceptors (cone arrestin^{+}) and horizontal expressed VGLUT2-tdTomato (calbindin^{+}), which seemed to suggest that VGLUT2 might not be a specific RGC marker in retina.[19] In addition, another study showed various expression of VGLUT2 in rat and human by antibody staining. VGLUT2 was present in horizontal cells and ganglion cells in rat and human retina, while it was also found in some amacrine cells in human retina.[20] Recently, RBPMS has been deemed as a whole RGC-specific marker, with one convincing reason being the almost complete colocalization of RBPMS^{+}/FG^{+} after retrograde FG administration.[7] However, there are no reports yet on generating RBPMS reporter knockin mice.

Reporter mice can be used to monitor the location and morphological changes of the reporter gene during development, as well as to study disease models caused by various experimental perturbations. They can also be used to estimate the effects of drug interventions, and as non-invasive imaging techniques for detecting pathological changes. Additionally, a naturally occurring Mgp reporter KI mouse has been used to study angiogenesis and glaucoma *in vivo*, from which researchers can observe retinal angiogenesis longitudinally.[21]

RBPMS is expressed in smooth muscle cells (SMCs), within transcriptionally downregulated during SMC dedifferentiation, and can be as a master regulator of alternative splicing in differentiated SMCs.[22] Recent research suggests that vascular SMCs and myofibroblasts control the

[1]State Key Laboratory of Ophthalmology, Zhongshan Ophthalmic Center, Sun Yat-sen University, Guangdong Provincial Key Laboratory of Ophthalmology and Visual Science, Guangzhou 510060, China
[2]Research Units of Ocular Development and Regeneration, Chinese Academy of Medical Sciences, Beijing 100730, China
[3]Lead contact
*Correspondence: zhyfeng@mail.sysu.edu.cn
https://doi.org/10.1016/j.isci.2023.108111

pathobiology of arteriolar choroidal neovascularization (CNV), as these cells infiltrate the lesion sites and form a support scaffold for endothelial cells, resulting in incomplete response to anti-VEGF therapy in neovascular age-related macular degeneration (AMD).[23] Therefore, it is speculated that RBPMS is not only a marker of RGCs, but also a potential target for choroid and retinal vascular treatment.

Here, we have created a new mouse strain in which the Cre recombinase gene was inserted into the RBPMS locus using CRISPR-Cas9 technology; the mice were crossed with Ai9 tdTomato reporter mice, resulting in the creation of RBPMS$^{CreERT2\text{-}tdTomato}$ mice, within the tdTomato protein fluorescence signals reflecting the endogenous expression of RBPMS accurately. We systematically examined the localization of RBPMS-tdTomato fluorescence signals at embryonic day 17.5 (E17.5) and in adult tissues, which demonstrated various tissue containing RBPMS-expressing cells. In addition, the tdTomato fluorescence signal was not only merely labeling RGCs, but also showed RBPMS protein in optic nerve, ciliary body, and retinal/choroidal vasculature. Furthermore, the strong fluorescence of tdTomato allows for non-invasive live imaging of RGCs and retinal/choroidal vasculature *in vivo*, providing a new tool for monitoring these cells and tissues over time.

RESULTS

Design and generation of RBPMS^{CreERT2} knockin mouse line by CRISPR-Cas9 strategy

To create a mouse line with a knockin of the CreERT2-P2A element at the translation initiation site of the first exon of the RBPMS gene, we used a CRISPR-Cas9 program without disrupting endogenous gene expression. This program involved the microinjection of sgRNA, a donor vector, and Cas9 into zygotes, which were then transplanted into pseudopregnant female mice. The resulting founder (F0) mice had the CreERT2-P2A sequence cassette inserted into exon 1 of RBPMS, as confirmed by the presence of homology arms (Figure 1A). These correctly targeted F0 mice were then crossed with wild-type (WT) C57 mice to produce the F1 generation.

We designed three RBPMS PCR primers, which were used to clone the 5′ arm, 3′ arm, and WT genes. The homozygous genotype was identified by the presence of only the two target fragments, while the heterozygous genotype was identified by the presence of both the two target fragments and one WT fragment (Figure 1B). The PCR results for mice 21, 23, 25, 26, 29, 31, and 32 showed the presence of 5′ arm, 3′ arm, and WT fragments, confirming that they were heterozygous RBPMS CreERT2-KI mice (Figures 1C–1E). To further confirm the insertion at the targeted site, the positive PCR products were analyzed by Sanger sequencing (Figure 1F).

The Ai9 reporter mouse used in this study contained a LoxP-flanked transcription termination cassette and expressed the tdTomato protein following Cre-mediated recombination (Figure S1A). This mouse was then crossed with RBPMSCreERT2 mice, resulting in the creation of double transgenic mice named RBPMS$^{CreERT2\text{-}tdTomato}$ mice, which will help to explore the endogenous RBPMS expression after tamoxifen induction (Figures S2B and S2C). To confirm the genotype of the RBPMS$^{CreERT2\text{-}tdTomato}$ mice, PCR was performed using targeting RBPMS-CreERT2 and CAG-tdTomato primers. The results showed that mice 107, 109, 111, and 112 were tdTomato homozygous and mouse 110 was tdTomato heterozygous, while all mice were CreERT2 heterozygous (Figures S2D and S2E).

Mapping of RBPMS expression in RBPMS$^{CreERT2\text{-}tdTomato}$ mouse embryo tissues

To evaluate the functionality of the RBPMS-CreERT2 and investigate RBPMS expression during embryonic development, we obtained double transgenic offspring at embryonic day 17.5 (E17.5) from pregnancy mice that had been induced with tamoxifen for 4 days. We performed immunofluorescent staining on embryo sections using an RBPMS antibody. The results showed that tdTomato fluorescence signals were co-expressed with RBPMS antibody in various tissues during embryogenesis and distributed throughout all three germ layers (Figure 2A).

As RBPMS is known as a marker of RGC, we observed the location of tdTomato-positive cells in the eye, which originates from the ectoderm. As expected, the RBPMS-tdTomato cells were mainly located in basal side of retina in multilayer structures in E17.5 embryo, and were co-located with the immunofluorescent staining signals. In addition, tdTomato fluorescence signals were also observed in the developing ciliary body and choroid (Figure 2B). Furthermore, sections revealed that many tdTomato-positive cells were located in brain zones, which are another ectoderm-originating tissue (Figure 2C). We observed strong fluorescence signals in mesoderm-derived tissues, including the heart and smooth muscle of blood vessels (Figures 2D and 2E), as well as in certain endoderm-derived tissues, such as the liver (Figure 2F), lung (Figure 2G), and intestine (Figure 2H). Our findings indicate that RBPMS is expressed in these tissue types.

RBPMS-tdTomato expression location in adult ocular tissue

In order to determine the expression pattern of the tdTomato protein in adult RBPMS$^{CreERT2\text{-}tdTomato}$ mice, the 3-months-old mice were treated with tamoxifen for consecutive 5 days before sampling. The expression levels of tdTomato were found to be low before exposure to tamoxifen-induced Cre recombinase; there were average less than 5% fluorescence leakage in retinal whole-mount and frozen sections, while most of the leaked fluorescence signals were not located in the ganglion cell layer (GCL) and optic nerve (Figures S2A and S2B).

Retinal whole-mount staining showed strong tdTomato fluorescence signals in the somata of RGCs and in the retinal vasculature (Figure S3A). Immunofluorescent staining showed that most of the tdTomato-positive RGCs colocalized with RBPMS (Figure S3B). The RBPMS-tdTomato expression was also analysis from eyeball and optic nerve frozen sections. The typical RBPMS-tdTomato positive RGC somata were arranged in a monolayer alignment in the basal retina, and significant tdTomato fluorescence signals were observed in the optic nerve, which is consistent with previous reports.[24,25] Additionally, some irregular shape tdTomato fluorescence signals were detected in the inner plexiform layer (IPL) and inner nuclear layer (INL), which were speculated to the dendrites of intrinsically photosensitive retinal ganglion cells according to literature reports.[26,27] In addition, tdTomato fluorescence signals were also detected in the choroidal vasculature and ciliary body, which has not been reported before (Figure 3A).

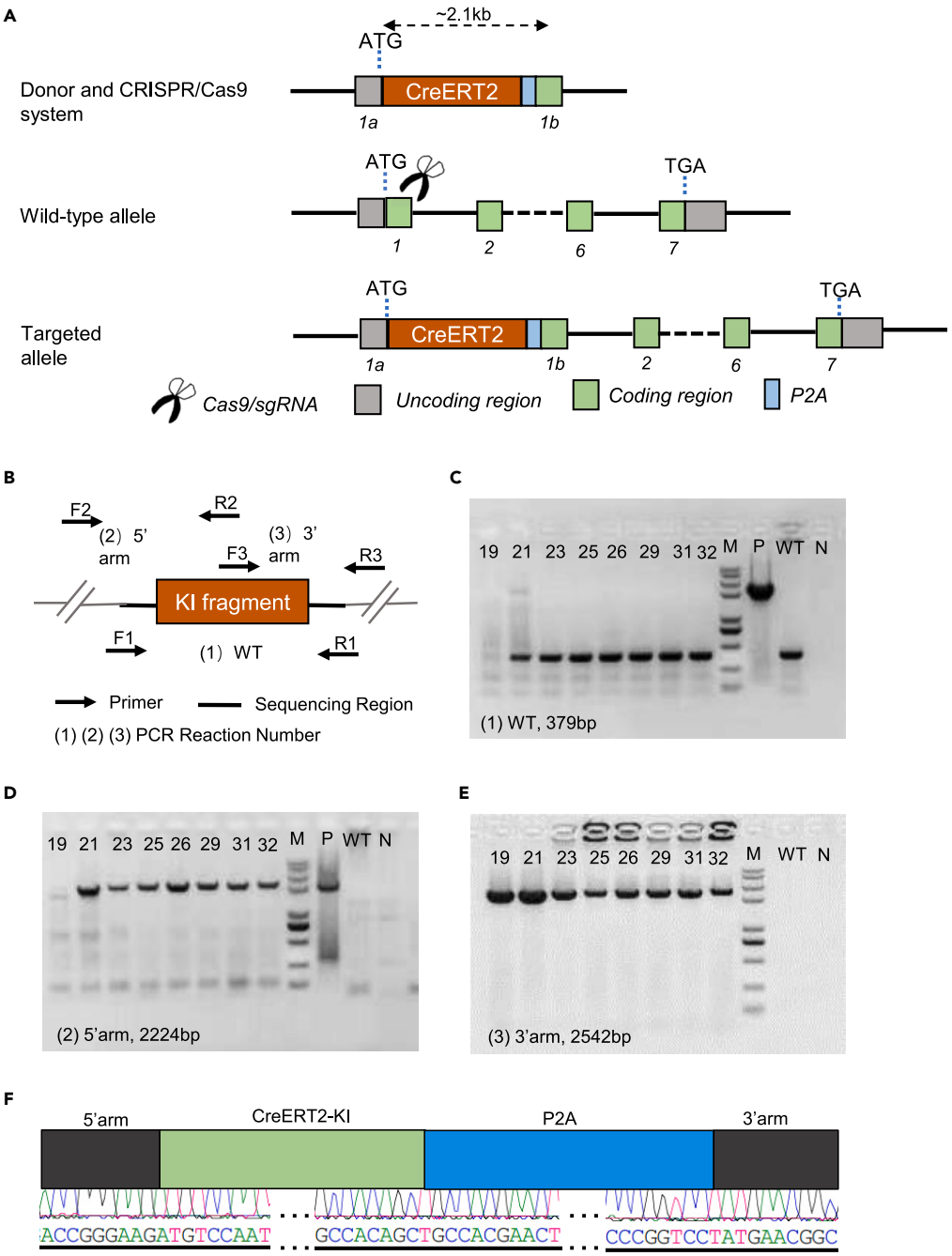

Figure 1. Design and generation of RBPMS^{CreERT2} knockin mouse line using the CRISPR-Cas9 strategy

(A) Diagram of RBPMS-WT, RBPMS-CreERT2 KI alleles, donor, and CRISPR-Cas9 system. Sequences containing CrtERT2-P2A gene cassette were inserted between the RBPMS translation initiation site ATG and the first exon coding region.

(B) The schematic of the PCR identification strategy. Primer 1 represents the WT allele, primer 2 represents the 5′ arm, and primer 3 represents the 3′ arm.

(C–E) PCR was performed on genomic DNA from the knockin founders with the designed primers. Two pairs of primers were used to confirm the knockin allele. WT: 379 bp, 5′ arm: 2224 bp, 3′ arm: 2542 bp.

(F) Sequences of the CrtERT2-P2A cassette boundaries. The green bar indicated the inserted CrtERT2 and the blue bar indicated the P2A.

Then, we observed the relationship between tdTomato fluorescence signals and a series of retinal makers using immunostaining analysis. Previous studies have reported that displaced amacrine cells make up nearly half of the neurons in the GCL.[28,29] Our analysis revealed that the majority of tdTomato-positive cells were co-located with RBPMS^{+} and Tuj1^{+} cells, accounting for 51% and 55% of GCL cells, respectively

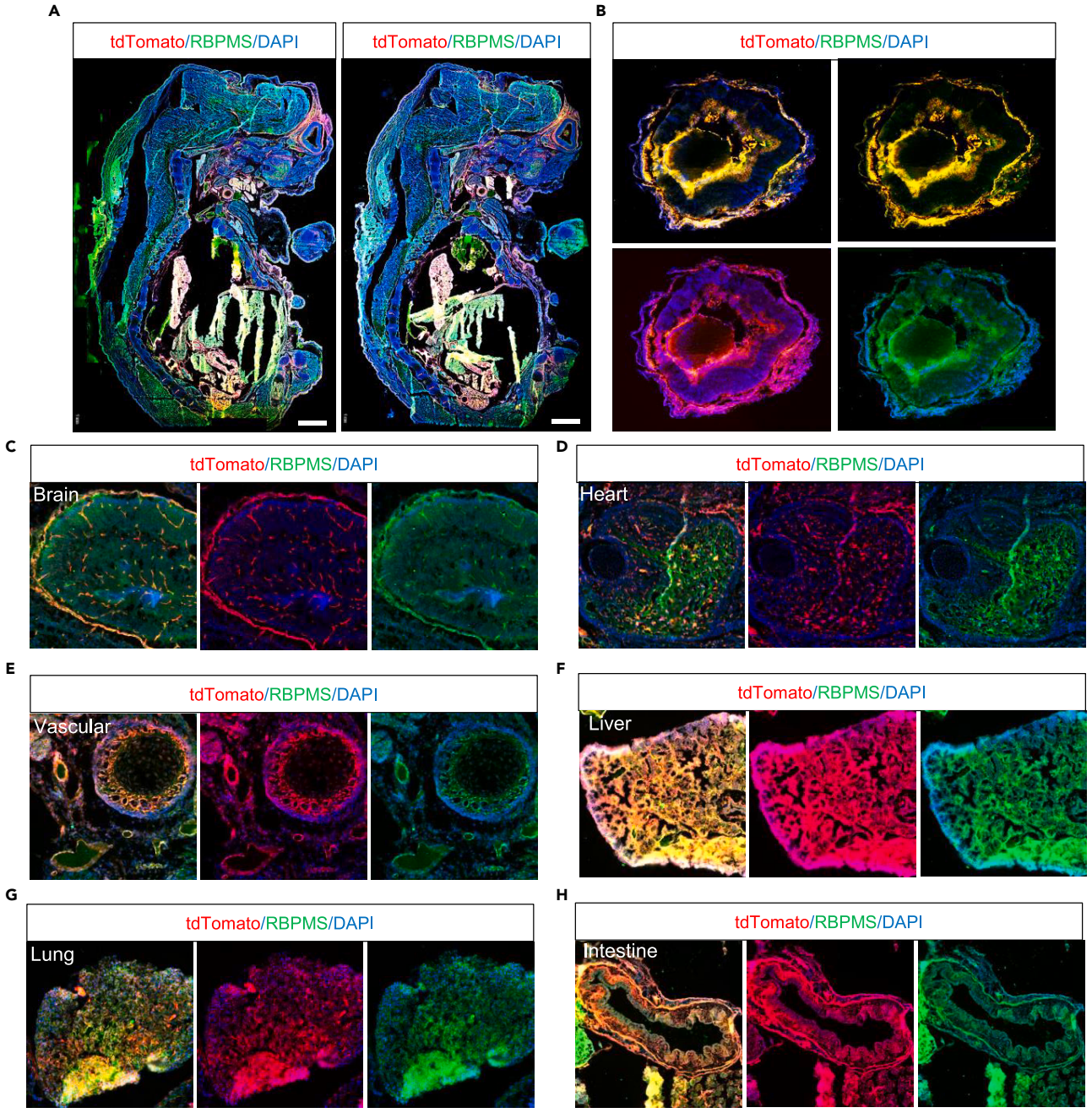

Figure 2. Mapping of RBPMS expression in RBPMS$^{CreERT2\text{-}tdTomato}$ mouse embryo tissues

(A) Images displaying tdTomato fluorescence signals and RBPMS immunofluorescence staining (GFP) of E17.5 embryo sections.

(B–H) Scale bar, 1 mm. Shown were representative images of tdTomato fluorescence signals from E17.5 embryo tissues within higher magnification in (B) eye, (C) brain, (D) heart, (E) vascular, (F) liver, (G) lung, and (H) intestine.

(Figures 3B–3E). Additionally, the immunostaining seemed to confirm that the majority of strong calretinin-positive fluorescence signals were located in the IPL while the outer nuclear layer (ONL) and GCL were found to distribute Calretinin^{+} tdTomato-placed and displaced amacrine cells, respectively. Additionally, there were nearly 20% of tdTomato-positive RGC expressing Calretinin in the GCL, as previously reported (Figures 3F and 3G).[30,31] The tdTomato fluorescence signals were also confirmed by immunofluorescent staining with tdTomato antibody (Figure 3H). Another type of interneuron, bipolar cells, located in the INL and linking the outer and inner retina, was immunostained with VSX2 and did not appear to co-locate with tdTomato fluorescence signals (Figure 3I). Photoreceptor cells, positive for the marker Recoverin, were found in the ONL and had hardly any tdTomato fluorescence signals (Figure 3J).

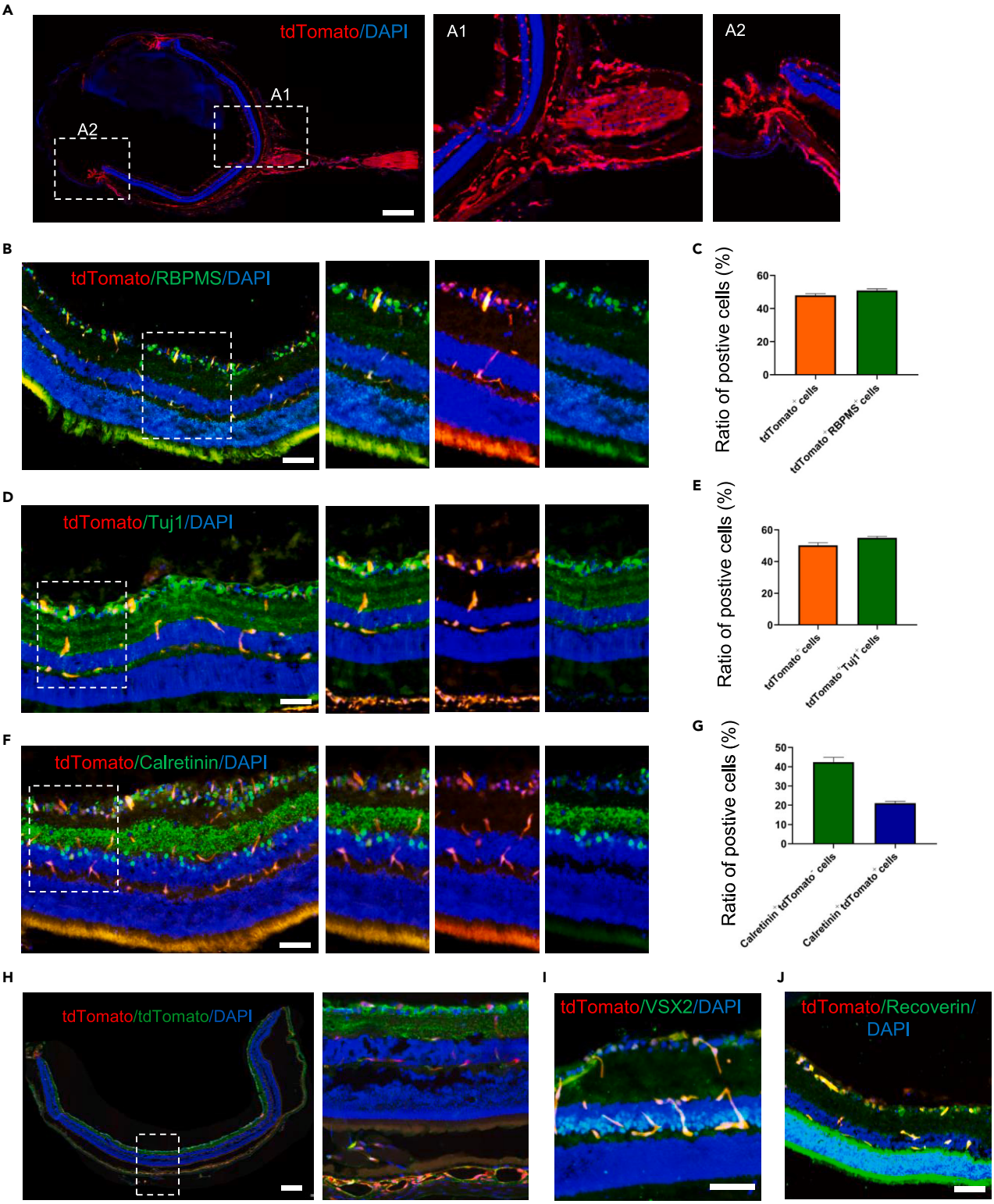

Figure 3. Expression of RBPMS in adult RBPMS$^{CreERT2\text{-}tdTomato}$ mouse ocular tissue

(A) Representative image of an adult mouse ocular frozen section after tamoxifen induction with strong tdTomato fluorescence signals present in the retinal ganglion layer (RGL), optic nerve, choroid vasculature and ciliary body. Scale bar, 500 μm.

Figure 3. *Continued*

(B and C) Ocular frozen sections labeled with RBPMS by immunofluorescent staining (green), and the ratio of tdTomato$^+$ and RBPMS$^+$ cells. Data are represented as mean ± SEM. Scale bar, 100 μm.

(D and E) Ocular frozen sections labeled with Tuj-1 by immunofluorescent staining (green), and the ratio of tdTomato$^+$ and Tuj-1$^+$ cells. Data are represented as mean ± SEM. Scale bar, 100 μm.

(F and G) Ocular frozen sections labeled with Calretinin by immunofluorescent staining (green), and the ratio of tdTomato$^+$ and Calretinin$^+$ cells. Data are represented as mean ± SEM. Scale bar, 100 μm.

(H) The ocular frozen sections were labeled with tdTomato by immunofluorescent staining (green). The right images show a higher magnification of the corresponding white box area. Scale bar, 100 μm.

(I) Ocular frozen sections were labeled with VSX2 by immunofluorescent staining (pseudo color green), Scale bar, 100 μm.

(J) The ocular frozen sections were labeled with Recoverin by immunofluorescent staining (green), Scale bar, 100 μm.

RBPMS-tdTomato-positive RGCs degenerated after optic nerve crush

In order to evaluate the reliability of tdTomato fluorescence signals and the utility of RBPMS$^{CreERT2\text{-}tdTomato}$ mice in research, the mice were subjected to an optic nerve crush procedure, which leads to degeneration of RGC soma and axons.[32] In normal retinal wholemounts, strong tdTomato fluorescence signals were observed in RGC cells and retinal blood vessels. However, nearly 70%–80% of the tdTomato-positive RGC somata died after optic nerve crushing for 12 days, just only about 5% survived, which were also observed in the CTB injection experiments (Figures 4A–4D). Additionally, frozen sections of the retina confirmed this phenomenon (Figure 4E). Immunofluorescent staining with Tuj1 and calretinin revealed that while RGC cells underwent apoptosis, calretinin$^+$ amacrine cells were preserved after ONC (Figures 4F and 4G). Additionally, tdTomato fluorescence signals in the optic nerve were also decreased following the ONC injury (Figure 4H). As expected, retinal and choroidal vasculature choroidal blood vessels were not affected by ONC injury and still had strong tdTomato fluorescence signals. These findings demonstrate that BPMS$^{CreERT2\text{-}tdTomato}$ mice can serve as a credible animal model for studying optic nerve injury or RGC degenerative diseases, such as glaucoma and optic neuropathy.

We also compared the efficiency of induction using tamoxifen before and after crushing the optic nerve. The results showed that there was no significant difference between the two (Figures S4A and S4B). The long-lasting stability of tdTomato expression may be a useful application for pregnant mice and disease models, as it avoids the negative effects of tamoxifen.

Laser-induced CNV in the RBPMS$^{CreERT2\text{-}tdTomato}$ mice

Previous study has established the relevance of the natural fluorescent properties of Mgp-tdTomato reporter mice in the detection of retinal vascular beds.[19] In a similar vein, we used OCT to examine the choroid and retinal vasculature of RBPMS$^{CreERT2\text{-}tdTomato}$ mice *in vivo*. The strong OCT angiography was able to detect the natural RBPMS-tdTomato fluorescence signals following tamoxifen induction, while there was no detectable signal without tamoxifen exposure (Figure 5A).

OCT angiography has been used to assess the status of CNV in clinical settings.[33] Therefore, we aimed to investigate the feasibility of using natural RBPMS-tdTomato fluorescence signals for longitudinal studies of the leakiness and proliferation of the choroidal bed in a non-invasive manner. Two groups of old and young RBPMS$^{CreERT2\text{-}tdTomato}$ mice were subjected to laser-induced burns at the same time. Both OCT-IR and fluorescein angiography mode were used to examine the area of photocoagulation 3, 7, and 12 days post laser induction. The results revealed prominent RBPMS-tdTomato fluorescence signals corresponding to the burns in old mice at 7 and 12 days *in vivo*, but no signals were observed in adult mice in this study (Figure 5B).

Beyond that, the RBPMS$^{CreERT2\text{-}tdTomato}$ mice eyeball frozen sections helped to recognize RBPMS-tdTomato-positive cells in the choroid vasculature, which were confirmed by immunostaining with α-SMA and PDGFR-β; the two markers were considered for labeling smooth muscle cells and pericytes (Figure 5C). Furthermore, the tdTomato-positive choroid vascular walls become thicker in CNV model than the normal choroid (Figure 5D). This phenomenon may represent a new pathology pattern of CNV, referred to as neovascular remodeling,[20] which could aid in the exploration of new therapeutic methods for wet AMD.

The characteristic of RBPMS expression in adult heart and cardiovascular tissues

Previous studies have highlighted the important role of RBPMS in cardiac mesoderm specification and binucleation as well as cardiovascular development, which confirmed that RBPMS not only showed high expression in the cardiomyocyte, but also mediated alternative mRNA splicing.[4,5] By means of RBPMS$^{CreERT2\text{-}tdTomato}$ mice, we could resolve the location and identify cell type of RBPMS-expressing cells from heart frozen sections and cultured heart cells/organoids. The frozen sections showed that RBPMS-tdTomato expression was widely distributed in myocardial cells and together with tdTomato, α-actinin, and cTnT expression, while were co-localized expression with α-SMA in cardiovascular smooth muscle cells (Figures 6A and 6B). Semi-quantitative PCR results showed the relative expression level of three isoforms, isoform 1 had the highest expression level, followed by isoform 4, while isoform 3 had the lowest expression level (Figure 6C). Considering the roles of RBPMS in heart development, we also explored whether the inserted CreER element could attenuate the downstream RBPMS expression; both of the PCR and western blot results showed that RBPMS expression levels had no obvious influence after tamoxifen induction in heart tissue (Figures 6D–6F).

As potential cardiac RBPMS$^+$ cell model, the natural cardiac organoids were generated from primary heart tissue which displayed visible tdTomato fluorescence (Figure 6G), and the organoid frozen sections showed that tdTomato fluorescence signals were co-expressed with

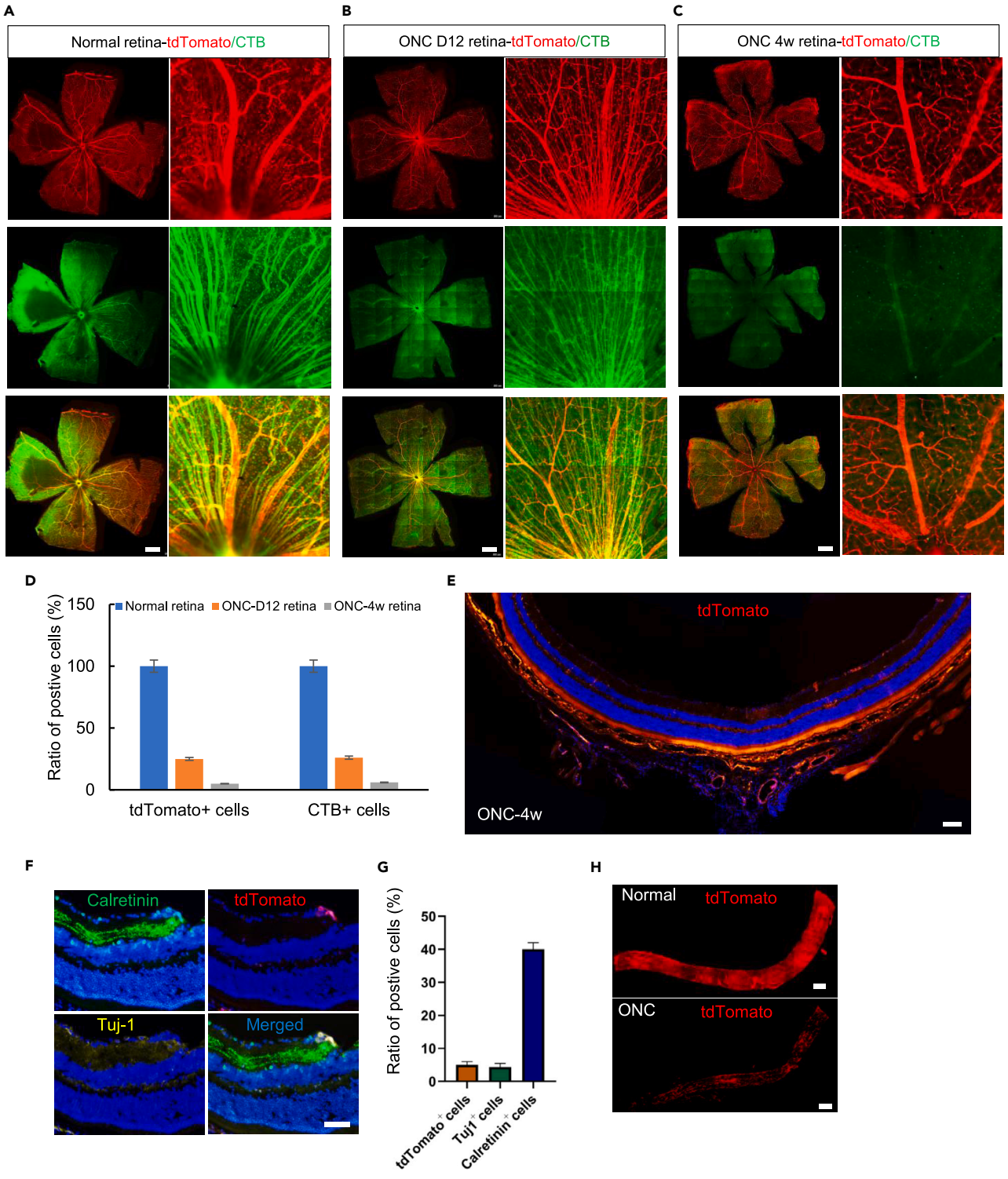

Figure 4. The degeneration of RBPMS-tdTomato$^+$ RGCs following optic nerve crush (ONC)

(A–C) Representative images from retinal wholemounts of normal adult mice after tamoxifen induction (A), mice within 12 days of an optic nerve crush (B), mice within 4 weeks of an optic nerve crush (C). CTB, green. The right images show a higher magnification of the corresponding white box area. Scale bar, 500 μm. (D) The ratio of tdTomato$^+$ and CTB$^+$ cells in normal and ONC retinal whole mounts. Data are represented as mean ± SEM.

Figure 4. *Continued*

(E) Representative image of an ONC adult mouse ocular frozen section. Scale bar, 100 μm.

(F–G) (F) ONC retina frozen sections labeled with calretinin (green) and Tuj-1 (yellow) by immunofluorescent staining, and (G) ratio of tdTomato$^+$, calretinin$^+$, and Tuj-1$^+$ cells. Data are represented as mean ± SEM. Scale bar, 100 μm.

(H) Optic nerves frozen sections of normal and ONC adult mice. Scale bar, 200 μm.

cTnT (Figure 6H). We also obtained RBPMS-tdTomato$^+$ cells by fluorescence-activated cell sorting; the adherent cultured live cells showed tdTomato fluorescence in cytoplasm within heterogeneous morphology, while isoform 1 had the highest expression level (Figures 6I–6K). Interestingly, the immunofluorescent staining showed that RBPMS were aggregating in the nucleus (Figure 6L).

Systematic analysis of the RBPMS expression in other adult tissues

Finally, we systematically examined the tdTomato fluorescence signals in various adult other tissues. The collected tissues were processed using frozen sections and the results showed that the brain, liver, lung, spleen, kidney, intestine, and bladder displayed various degree tdTomato fluorescence signals (Figures S5A–S5G). These various adult tissues frozen sections were also counterstaining with RBPMS and tdTomato (Figures 7A–7G and S7). The results showed that RBPMS were extensive expression in liver, spleen, lung, and kidney, as well as the smooth muscle cells enriching tissues, such as intestine and bladder which were counterstaining with α-SMA; while the brain had the fewest RBPMS expression, the smooth muscle cells and pericyte of vascular were identified by α-SMA and PDGFR-β.

Then, we investigated the three RBPMS isoforms and protein expression levels among these tissues, bladder had the highest expression level and brain expressing the lowest; lung, kidney, and liver also had relative high expression comparing to brain (Figures 7H–7J). In addition, we also analyzed the RBPMS gene and protein expression levels before and after tamoxifen induction; the results showed most of the tissues had no or mild decreased expression, but the lung showed obvious decreased expression (Figures S6A–S6C).

DISCUSSION

In this study, we established a tamoxifen-inducible transgenic mouse model. The CreERT2 gene was inserted after the ATG signal of RBPMS, enabling us to spatiotemporally monitor RBPMS expression in cells from embryogenesis to adulthood. To obtain specific RBPMS-tdTomato fluorescence signals *in vivo*, we crossed the transgenic mice with Ai9 mice that contain the Rosa-CAG-LSL-tdTomato-WPRE conditional allele. The resulting double transgenic mice, named RBPMS$^{CreERT2\text{-}tdTomato}$, could provide precise RBPMS expressing cell origin and lineage tracing, as well as serve as a disease model for various interventions. Furthermore, this model allows for non-invasive assessment of disease progression *in vivo* over a long period of time and isolation of specific RBPMS-tdTomato-positive cells for cell model or molecular bioinformatics analysis.

There were several advantages of using our conditionally induced RBPMS$^{CreERT2\text{-}tdTomato}$ mice. First, CreER2 is a fusion protein of Cre and a modified estrogen receptor, which prevents Cre from entering the nucleus until tamoxifen induction is applied. This switch element is commonly used for lineage tracing, conditional gene knockout, and functional studies of lethal genes. However, some issues with this technique include reporter background leakage that is not dependent on tamoxifen and variations among different reporters.[34] Second, we chose to cross the Ai9 mouse line to screen for RBPMS$^{CreERT2\text{-}tdTomato}$ mice. The Ai9 line is considered a valuable tool for specifically labeling target cells, as it is more specific than other reporter lines such as Ai14.[35] We also checked for fluorescent signal background leakage in ocular tissues without administering tamoxifen and found that there were only a few sporadic tdTomato fluorescent signals in the retina, with hardly any signals in the retinal/choroid vasculature and ciliary body. The RBPMS-expressing cells showed a significant difference in tdTomato fluorescent signals with and without tamoxifen administration (Figure S1). Third, the Ai9 line has an att site-flanked *neo* selection cassette at the 3′ end of the targeted allele. RBPMS$^{CreERT2\text{-}tdTomato}$ mice can be used as a donor line to generate new transgenic mice when crossed with flox mice containing *loxP* sites flanking the essential exons of the target genes, allowing for time-controlled conditional knockout for loss-of-function studies.[36]

In order to confirm the validity of lineage tracing CreERT2-labeled populations, we examined the RBPMS-tdTomato fluorescent signals in embryos. Tamoxifen has been known to have negative effects on placental and embryonic development, making the timing and dosage of exposure crucial. Previous studies have shown that administering tamoxifen earlier than E8.5 or at a dosage greater than 50 mg/kg can lead to embryotoxicity and birth defects.[37,38] Taking these findings into consideration, we chose a dosage of 75 mg/kg for inducing Cre activity[39] and began tamoxifen exposure at E10.5. This strategy allowed us to obtain embryonic tissues with strong and clear RBPMS-tdTomato fluorescent signals without causing abortion or embryotoxicity.

The sections of the entire embryo, akin to a valuable library, contain a wealth of information on the distribution of RBPMS-tdTomato-positive cells across triploblastic tissues. Of particular interest was the ocular tissue, as the embryonic sections of the eyeball accurately depicted multilayer RBPMS-tdTomato-positive RGCs distributed in the basal retina. Additionally, strong tdTomato fluorescent signals were observed in the ciliary body, choroidal vessels, and the periphery of the lens vesicle, which had not been reported previously. As RBPMS can serve as a marker of SMC, the presence of these signals in these areas can likely be explained by the lack of suitable models for research. However, further verification is needed to determine the specific cell type and function of RBPMS-expressing cells in the ciliary body and lens vesicle. Non-ocular tissues were also examined for tdTomato fluorescent signals. Immunohistochemical staining revealed the presence of tdTomato-positive cells in the brain, heart, lung, liver, and intestine, with co-localization with RBPMS.

The most important finding of this study is that we have proven that the GCL tdTomato-positive cells are indeed RGCs. The GCL layer is composed of over 90% RGCs and displaced amacrine cells, which are highly interconnected synaptically.[29] Our results from section analysis

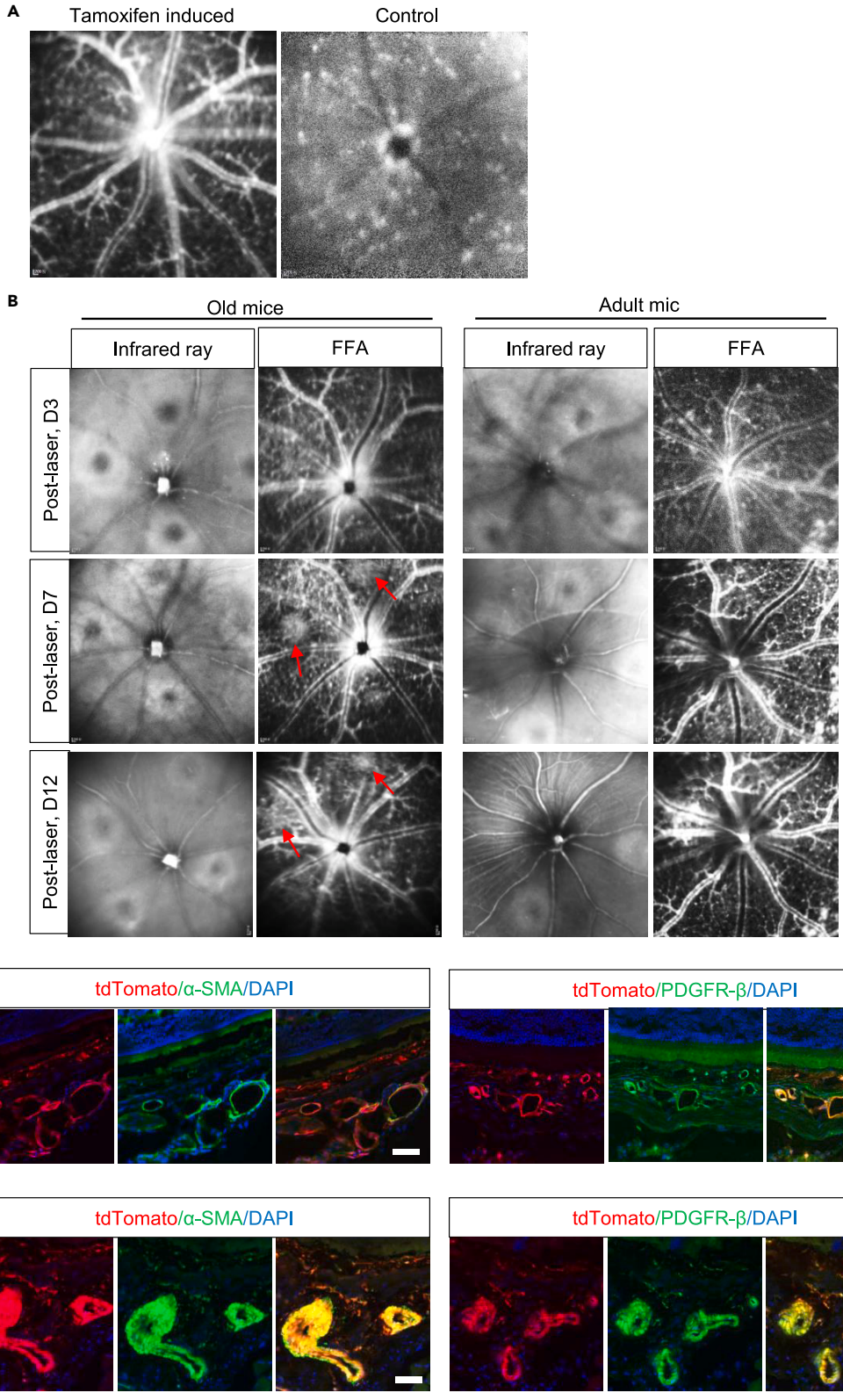
A
Tamoxifen induced
Control
B
Old mice
Adult mic
Infrared ray
FFA
Infrared ray
FFA
Post-laser, D3
Post-laser, D7
Post-laser, D12
C
tdTomato/α-SMA/DAPI
tdTomato/PDGFR-β/DAPI
D
tdTomato/α-SMA/DAPI
tdTomato/PDGFR-β/DAPI

Figure 5. Laser-induced CNV in the RBPMS$^{CreERT2\text{-}tdTomato}$ mice

(A) Noninvasive images of the retinal/choroid vasculature with and without tamoxifen induction.

(B) OCT-IR and FFA photo mode taken from live mice at 3, 7, and 12 days post laser photocoagulation. These representative images were captured from the same eye of a single mouse. FFA images dipict the natural tdTomato fluorescence signals, with the focus on the vessel wall. Red arrow indicates the presence of tdTomato-labeled neovascularization after CNV has occurred.

(C) The normal ocular frozen sections were labeled with α-SMA and PDGFR-β by immunofluorescent staining (green), respectively. Scale bars, 50 μm.

(D) The CNV model ocular frozen sections were labeled with α-SMA and PDGFR-β by immunofluorescent staining (green). Scale bars, 50 μm.

showed that nearly all of the tdTomato-positive cells co-localized with RBPMS by immunohistochemical staining. Additionally, while the stained RBPMS were mainly distributed in the GCL layer, RBPMS-tdTomato fluorescent signals were also seen in dendrites extending into the IPL and nerve fiber layer. This suggests that the natural RBPMS-tdTomato indicator may provide more information than indirect staining methods. To eliminate confusion with displaced amacrine cells, we analyzed the location and proportion of tdTomato and calretinin-positive cells. The immunoreactive results showed that almost all of them did not co-localize, with less than 20% of double-positive cells being considered calretinin-positive RGCs.[40] As expected, there were strong tdTomato fluorescent signals in the optic nerve, which helps to establish an RGC/optic nerve injury disease model. Previous studies have shown that approximately 80% of RGCs die within 2 weeks, within one slower speed degeneration subsequent time.[41,42] RBPMS$^{CreERT2\text{-}tdTomato}$ mice were operated on for an optic nerve crush operation, and both the whole retina and sections revealed that more than 90% of RGCs somas and axons disappeared after 4 weeks. However, calretinin-positive amacrine cells seemed to have not been affected, which is consistent with previous reports. This may be another piece of evidence for RGC authentication.

The development of reporter mice and the ability to image the dynamics of individual cell and tissue processes in living animals has sparked great interest in the field. These techniques have been applied to observe astrogliosis, microglial activation, endoplasmic reticulum stress, and retinal angiogenesis.[43–46] Compared to traditional measurement methods, the new model overcomes defects such as repeated fluorescein dye injection, short circulation time, and discreteness, and improves experimental repeatability and the ability to acquire identical, long-term data without causing stress to animals. The use of tdTomato-positive SMCs in the retinal and choroidal vasculature has been determined as a way to monitor the progress and outcome of AMD *in vivo*, which addresses the shortage of fluorescent vascular retina. In addition to capillary neovascularization, arteriolarization and perivascular fibrosis may also be risk factors for intraocular pressure elevation and poor outcomes in AMD. The term "neovascular remodeling" illustrates that SMCs and myofibroblasts control the pathological mechanism and result in an incomplete response to anti-VEGF therapy.[20] Live-imaging of RBPMS-tdTomato^{+} SMCs provides new targets for pathological exploration and drug screening.

Our research revealed that RBPMS-tdTomato fluorescent signals are present in various adult organs, including the brain, heart, lung, kidney, liver, and spleen. The distribution of these signals varies among the organs, with a dispersed and widespread pattern in the heart and spleen, a concentrated distribution around tubular structures in the lung and liver, and strong fluorescent signals in the glomerulus. Although we have not yet fully understood the characteristics of RBPMS^{+} cells in these non-ocular tissues, we believe that these organs provide a wealth of cell models for exploring the function of RBPMS in different physical environments. To further investigate this, we established 2D monolayer and 3D organoids culture systems using primary heart, lung, kidney, and spleen cells/tissues. We observed that RBPMS proteins are located in the nucleus, perinuclear region, and cytoplasm in various types of cells. Together with the various subcellular localization and morphology observed in whole embryo sections, we speculate that these different patterns may represent specific molecular functions.

RBPMS, or RNA-binding proteins with multiple splicing, have been shown to play a role as a splicing regulator and can affect the expression of certain actively transcribed genes. Their functions vary depending on their subcellular localization; for example, in the cytoplasm, they are responsible for stability and transport,[47] while in the mitochondria and nucleus they play a role in the selection of germline RNAs for localization in the germ plasm.[48] The splicing regulation provided by RBPMS has been found to modulate the phenotypic switch between constriction and proliferation in SMCs.[49] Additionally, RBPMS have been shown to balance synaptogenesis and axon arborization in RGCs by interacting with other RNA-binding proteins, and to negatively control the translation of the guidance cue receptor Neuropolin-1 in RGCs using a zebrafish model.[50,51] However, research on the role of RBPMS in the regulation of retinal development and RGC axon topology construction in mammals is limited. Our RBPMS$^{CreERT2\text{-}tdTomato}$ mice will provide one animal model to fill this gap in understanding.

In summary, we present a mouse model, the RBPMS-Cre knockin mouse, which when crossed with a tdTomato reporter strain results in the RBPMS$^{CreERT2\text{-}tdTomato}$ mice. These mice allow for the identification of RBPMS-positive cells in ocular and non-ocular tissues throughout development, from embryo to adulthood. Our model not only accurately labels RGCs, but also reveals new RBPMS-expressing cells in the ciliary body and retinal/choroid vasculature. This mouse model has several potential future applications, including the isolation of RBPMS^{+} cells for use in cell models, the exploration of endogenous RGC regeneration factors, the screening of new therapeutic methods for wet AMD, and the investigation of the mechanism of RBPMS splicing regulation in retinal development and disease.

Limitations of the study

We just uncovered part of the RBPMS-tdTomato cell types, such as RGC, myocardium, pericytes, vascular smooth muscle cells, and smooth muscle-enriched tissues; there were also some other RBPMS+ cell types in liver, lung, and so on, that would be worthwhile to be investigated in further studies. Although RBPMS$^{CreERT2\text{-}tdTomato}$ mouse line can trace and identify RGCs clearly, we have not established a protocol to digest the tdTomato-based RBPMS^{+} RGCs in the current study.

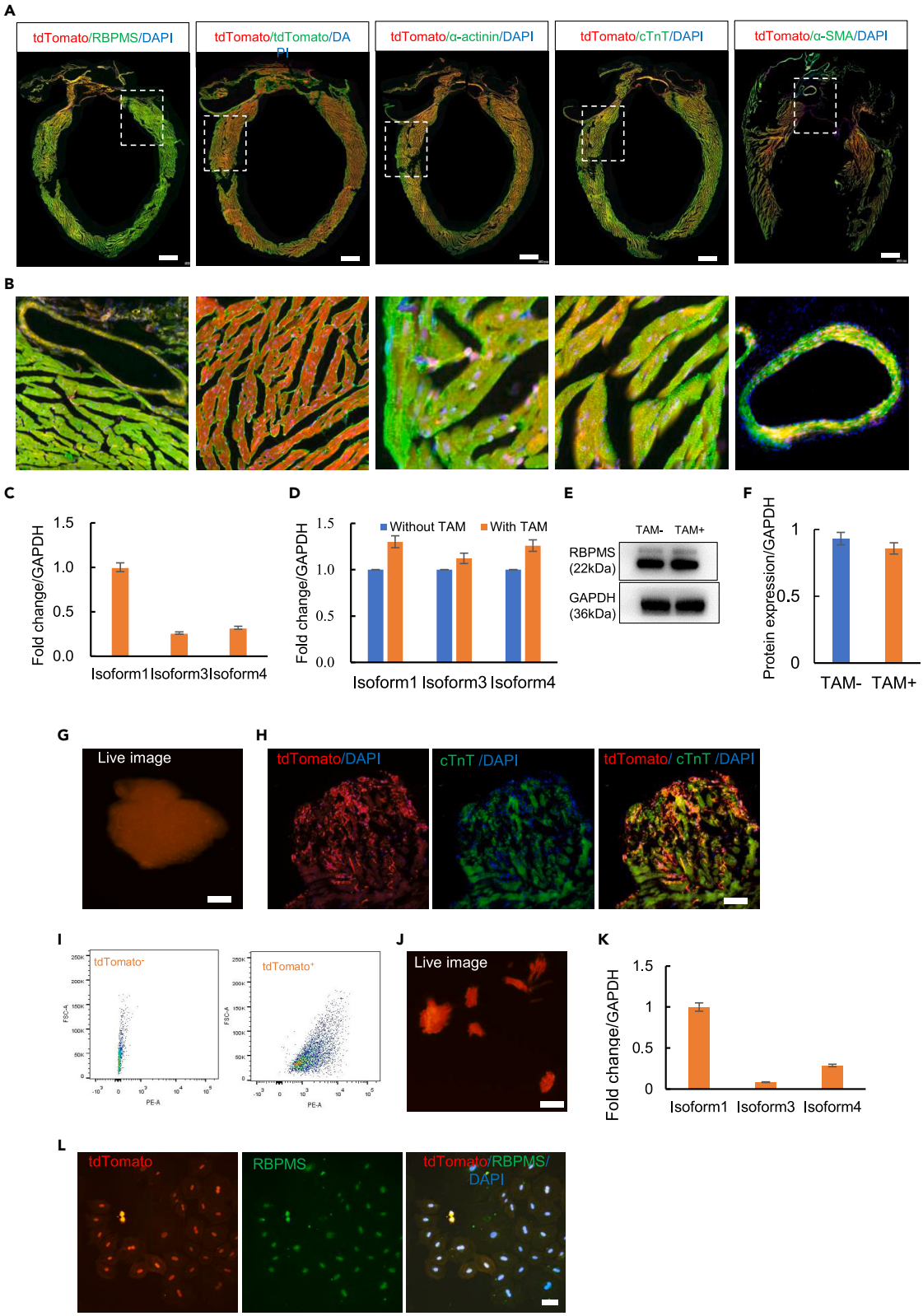
A
tdTomato/RBPMS/DAPI
tdTomato/tdTomato/DAPI
tdTomato/α-actinin/DAPI
tdTomato/cTnT/DAPI
tdTomato/α-SMA/DAPI
B
C
Fold change/GAPDH
1.5
1.0
0.5
0.0
Isoform1 Isoform3 Isoform4
D
Without TAM
With TAM
Fold change/GAPDH
Isoform1 Isoform3 Isoform4
E
TAM- TAM+
RBPMS (22kDa)
GAPDH (36kDa)
F
Protein expression/GAPDH
1
0.5
0
TAM- TAM+
G
Live image
H
tdTomato/DAPI
cTnT /DAPI
tdTomato/ cTnT /DAPI
I
tdTomato-
tdTomato+
FSC-A
PE-A
J
Live image
K
Fold change/GAPDH
1.5
1
0.5
0
Isoform1 Isoform3 Isoform4
L
tdTomato
RBPMS
tdTomato/RBPMS/DAPI

Figure 6. The characteristic of RBPMS in adult heart and cardiovascular

(A) Representative images of adult heart frozen sections for immunofluorescence staining with RBPMS (green), tdTomato (green), α-actinin (green), cTnT (green), and α-SMA (green) (B) show a higher magnification of the corresponding white box area in (A). Scale bar, 500 μm.

(C) qRT-PCR analysis of RBPMS-isoform1, isoform3, and isoform4 expression in adult heart tissues. Data are represented as mean ± SEM.

(D) qRT-PCR analysis of RBPMS expression levels after TAM induction in adult heart tissues. Data are represented as mean ± SEM.

(E and F) WB analysis of RBPMS expression levels after TAM induction in adult heart tissues. Data are represented as mean ± SEM.

(G) Images of cultured live cells from primary heart tissues. Scale bar, 200 μm.

(H) Immunofluorescent staining performed on heart organoids cTnT (green). Scale bar, 200 μm.

(I) FACS-based cell sorting by tdTomato fluorescence signal.

(J) Representative image of cultured live cells from primary heart tissues. Scale bar, 200 μm.

(K) qRT-PCR analysis of RBPMS-isoform1, isoform3, and isoform4 expression in cultured heart cells. Data are represented as mean ± SEM.

(L) Immunofluorescent staining of adherent heart cells using RBPMS (green). The right images show a higher magnification of the corresponding white box area. Scale bar, 200 μm.

STAR★METHODS

Detailed methods are provided in the online version of this paper and include the following:

- KEY RESOURCES TABLE
- RESOURCE AVAILABILITY
  - Lead contact
  - Materials availability
  - Data and code availability
- EXPERIMENTAL MODEL AND STUDY PARTICIPANT DETAILS
  - Generation of mouse line
  - Optic nerve crush (ONC)
  - Laser-induced choroidal neovascularization (CNV) and OCT-angiography
- METHOD DETAILS
  - Genotyping verification by PCR and DNA sequence
  - Tamoxifen induction
  - Tissue preparation and immunohistochemistry fluorescence staining
  - The primary heart cells culture and tdTomato-based FACS sorting
  - qRT-PCR
  - Western blot
- QUANTIFICATION AND STATISTICAL ANALYSIS

SUPPLEMENTAL INFORMATION

Supplemental information can be found online at https://doi.org/10.1016/j.isci.2023.108111.

ACKNOWLEDGMENTS

The authors thank Professor Chunqiao Liu for allowing generous access to his OCT instrumentation, and also thank the members of GemPharmatech (China) for assisting generation of the RBPMS$^{CreERT2\text{-}KI}$ mouse strain. We also thank Professor Qiuling Xiang for kindly offering α-actinin and cTnT antibodies.

This study was funded by the National Natural Science Foundation of China (81721003), Local Innovative and Research Teams Project of Guangdong Pearl River Talents Program (2017BT01S138), CAMS Innovation Fund for Medical Sciences (2019-I2M-5-005), and the State Key Laboratory of Ophthalmology, Zhongshan Ophthalmic Center, Sun Yat-sen University.

AUTHOR CONTRIBUTIONS

G.L. and Y.Z. conceptualized the study. Y.Z. and Y.L. supervised the study. G.L., Y.T.L., Q.Z., and W.C. performed the experiments. K.L. performed the CNV mice model. The manuscript was written by G.L. and Y.Z.

DECLARATION OF INTERESTS

The authors declare no competing interests.

INCLUSION AND DIVERSITY

We support inclusive, diverse, and equitable conduct of research.

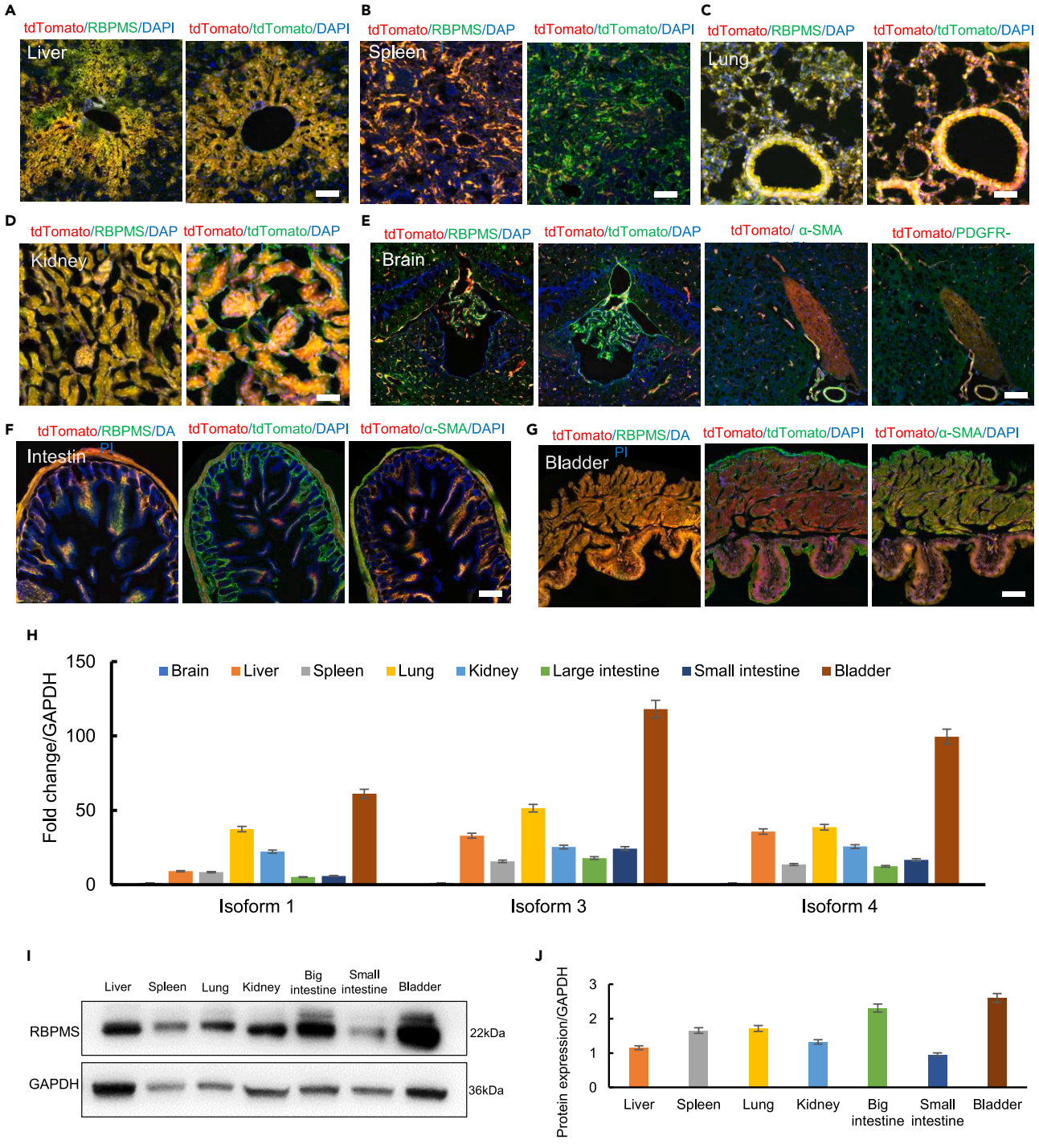

Figure 7. Systematic analysis the RBPMS expression in adult other tissues

(A–G) The representative RBPMS and tdTomato counterstaining images of adult tissues: (A) liver, (B) spleen, (C) lung, (D) kidney, (E) brain, the sections were also immunofluorescence staining with α-SMA (green) and PDGFR-β (green), (F) intestine, the sections were also immunofluorescence staining with α-SMA (green) (G) bladder, the sections were also immunofluorescence staining with α-SMA (green). Scale bars, 100 μm.

(H) qRT-PCR analysis of RBPMS-isoform1, isoform3, and isoform4 expression levels among the various tissues, comparing to the brain.

(I and J) WB analysis of RBPMS protein expression levels among the various tissues. Data are represented as mean ± SEM.

Received: May 30, 2023
Revised: August 27, 2023
Accepted: September 28, 2023
Published: October 2, 2023

REFERENCES

1. Maris, C., Dominguez, C., and Allain, F.H.T. (2005). The RNA recognition motif, a plastic RNA-binding platform to regulate post-transcriptional gene expression. FEBS J. *272*, 2118–2131. https://doi.org/10.1111/j.1742-4658.2005.04653.x.
2. Wilmore, H.P., McClive, P.J., Smith, C.A., and Sinclair, A.H. (2005). Expression profile of the RNA-binding protein gene hermes during chicken embryonic development. Dev. Dyn. *233*, 1045–1051. https://doi.org/10.1002/dvdy.20392.
3. Farazi, T.A., Leonhardt, C.S., Mukherjee, N., Mihailovic, A., Li, S., Max, K.E.A., Meyer, C., Yamaji, M., Cekan, P., Jacobs, N.C., et al. (2014). Identification of the RNA recognition element of the RBPMS family of RNA-binding proteins and their transcriptome-wide mRNA targets. RNA *20*, 1090–1102. https://doi.org/10.1261/rna.045005.114.
4. Bartsch, D., Kalamkar, K., Ahuja, G., Lackmann, J.W., Hescheler, J., Weber, T., Bazzi, H., Clamer, M., Mendjan, S., Papantonis, A., and Kurian, L. (2023). mRNA translational specialization by RBPMS presets the competence for cardiac commitment in hESCs. Sci. Adv. *9*, eade1792. https://doi.org/10.1126/sciadv.ade1792.
5. Gan, P., Wang, Z., Morales, M.G., Zhang, Y., Bassel-Duby, R., Liu, N., and Olson, E.N. (2022). RBPMS is an RNA-binding protein that mediates cardiomyocyte binucleation and cardiovascular development. Dev. Cell *57*, 959–973.e7. https://doi.org/10.1016/j.devcel.2022.03.017.
6. Kwong, J.M.K., Caprioli, J., and Piri, N. (2010). RNA binding protein with multiple splicing: a new marker for retinal ganglion cells. Invest. Ophthalmol. Vis. Sci. *51*, 1052–1058. https://doi.org/10.1167/iovs.09-4098.
7. Rodriguez, A.R., de Sevilla Müller, L.P., and Brecha, N.C. (2014). The RNA binding protein RBPMS is a selective marker of ganglion cells in the mammalian retina. J. Comp. Neurol. *522*, 1411–1443. https://doi.org/10.1002/cne.23521.
8. Marchesi, N., Fahmideh, F., Boschi, F., Pascale, A., and Barbieri, A. (2021). Ocular Neurodegenerative Diseases: Interconnection between Retina and Cortical Areas. Cells *10*, 2394. https://doi.org/10.3390/cells10092394.
9. Kerrison, J.B., Duh, E.J., Yu, Y., Otteson, D.C., and Zack, D.J. (2005). A system for inducible gene expression in retinal ganglion cells. Invest. Ophthalmol. Vis. Sci. *46*, 2932–2939. https://doi.org/10.1167/iovs.04-1237.
10. Campsall, K.D., Mazerolle, C.J., De Repentingy, Y., Kothary, R., and Wallace, V.A. (2002). Characterization of transgene expression and Cre recombinase activity in a panel of Thy-1 promoter-Cre transgenic mice. Dev. Dyn. *224*, 135–143. https://doi.org/10.1002/dvdy.10092.
11. Parmhans, N., Fuller, A.D., Nguyen, E., Chuang, K., Swygart, D., Wienbar, S.R., Lin, T., Kozmik, Z., Dong, L., Schwartz, G.W., and Badea, T.C. (2021). Identification of retinal ganglion cell types and brain nuclei expressing the transcription factor Brn3c/Pou4f3 using a Cre recombinase knock-in allele. J. Comp. Neurol. *529*, 1926–1953. https://doi.org/10.1002/cne.25065.
12. Ge, Y., Wu, F., Cheng, M., Bard, J., and Mu, X. (2020). Two new genetically modified mouse alleles labeling distinct phases of retinal ganglion cell development by fluorescent proteins. Dev. Dyn. *249*, 1514–1528. https://doi.org/10.1002/dvdy.233.
13. Miltner, A.M., Mercado-Ayon, Y., Cheema, S.K., Zhang, P., Zawadzki, R.J., and La Torre, A. (2019). A Novel Reporter Mouse Uncovers Endogenous Brn3b Expression. Int. J. Mol. Sci. *20*, 2903. https://doi.org/10.3390/ijms20122903.
14. Zheng, D., Yang, X., Sheng, D., Yu, D., Liang, G., Guo, L., Xu, M., Hu, X., He, D., Yang, Y., et al. (2016). Pou4f2-GFP knock-in mouse line: A model for studying retinal ganglion cell development. Genesis *54*, 534–541. https://doi.org/10.1002/dvg.22960.
15. Reif, A.E., and Allen, J.M. (1964). The AKR thymic antigen and its distribution in leukemias and nervous tissues. J. Exp. Med. *120*, 413–433. https://doi.org/10.1084/jem.120.3.413.
16. Morris, R. (1985). Thy-1 in developing nervous tissue. Dev. Neurosci. *7*, 133–160. https://doi.org/10.1159/000112283.
17. Barnstable, C.J., and Dräger, U.C. (1984). Thy-1 antigen: a ganglion cell specific marker in rodent retina. Neuroscience *11*, 847–855. https://doi.org/10.1016/0306-4522(84)90195-7.
18. Feng, G., Mellor, R.H., Bernstein, M., Keller-Peck, C., Nguyen, Q.T., Wallace, M., Nerbonne, J.M., Lichtman, J.W., and Sanes, J.R. (2000). Imaging neuronal subsets in transgenic mice expressing multiple spectral variants of GFP. Neuron *28*, 41–51. https://doi.org/10.1016/s0896-6273(00)00084-2.
19. Wang, L., Klingeborn, M., Travis, A.M., Hao, Y., Arshavsky, V.Y., and Gospe, S.M., 3rd (2020). Progressive optic atrophy in a retinal ganglion cell-specific mouse model of complex I deficiency. Sci. Rep. *10*, 16326. https://doi.org/10.1038/s41598-020-73353-0.
20. Gong, J., Jellali, A., Mutterer, J., Sahel, J.A., Rendon, A., and Picaud, S. (2006). Distribution of vesicular glutamate transporters in rat and human retina. Brain Res. *1082*, 73–85. https://doi.org/10.1016/j.brainres.2006.01.111.
21. Asokan, P., Mitra, R.N., Periasamy, R., Han, Z., and Borrás, T. (2018). A Naturally Fluorescent Mgp Transgenic Mouse for Angiogenesis and Glaucoma Longitudinal Studies. Invest. Ophthalmol. Vis. Sci. *59*, 746–756. https://doi.org/10.1167/iovs.17-22992.
22. Nakagaki-Silva, E.E., Gooding, C., Llorian, M., Jacob, A.G., Richards, F., Buckroyd, A., Sinha, S., and Smith, C.W.J. (2019). Identification of RBPMS as a mammalian smooth muscle master splicing regulator via proximity of its gene with super-enhancers. Elife *8*, e46327. https://doi.org/10.7554/eLife.46327.
23. Mettu, P.S., Allingham, M.J., and Cousins, S.W. (2021). Incomplete response to Anti-VEGF therapy in neovascular AMD: Exploring disease mechanisms and therapeutic opportunities. Prog. Retin. Eye Res. *82*, 100906. https://doi.org/10.1016/j.preteyeres.2020.100906.
24. Nadal-Nicolás, F.M., Galindo-Romero, C., Lucas-Ruiz, F., Marsh-Amstrong, N., Li, W., Vidal-Sanz, M., and Agudo-Barriuso, M. (2023). Pan-retinal ganglion cell markers in mice, rats, and rhesus macaques. Zool. Res. *44*, 226–248. https://doi.org/10.24272/j.issn.2095-8137.2022.308.
25. Pereiro, X., Ruzafa, N., Urcola, J.H., Sharma, S.C., and Vecino, E. (2020). Differential Distribution of RBPMS in Pig, Rat, and Human Retina after Damage. Int. J. Mol. Sci. *21*, 9330. https://doi.org/10.3390/ijms21239330.
26. Johnson, E.N., Westbrook, T., Shayesteh, R., Chen, E.L., Schumacher, J.W., Fitzpatrick, D., Field, G.D., and Field, G.D. (2019). Distribution and diversity of intrinsically photosensitive retinal ganglion cells in tree shrew. J. Comp. Neurol. *527*, 328–344. https://doi.org/10.1002/cne.24377.
27. Chen, C.K., Kiyama, T., Weber, N., Whitaker, C.M., Pan, P., Badea, T.C., Massey, S.C., Mao, C.A., and Mao, C. (2021). Characterization of Tbr2-expressing retinal ganglion cells. J. Comp. Neurol. *529*, 3513–3532. https://doi.org/10.1002/cne.25208.
28. Akopian, A., Kumar, S., Ramakrishnan, H., Viswanathan, S., and Bloomfield, S.A. (2019). Amacrine cells coupled to ganglion cells via gap junctions are highly vulnerable in glaucomatous mouse retinas. J. Comp. Neurol. *527*, 159–173. https://doi.org/10.1002/cne.24074.
29. Schlamp, C.L., Montgomery, A.D., Mac Nair, C.E., Schuart, C., Willmer, D.J., and Nickells, R.W. (2013). Evaluation of the percentage of ganglion cells in the ganglion cell layer of the rodent retina. Mol. Vis. *19*, 1387–1396.
30. Kovács-Öller, T., Szarka, G., Tengölics, Á.J., Ganczer, A., Balogh, B., Szabó-Meleg, E., Nyitrai, M., and Völgyi, B. (2020). Spatial Expression Pattern of the Major Ca2+-Buffer Proteins in Mouse Retinal Ganglion Cells. Cells *9*, 792. https://doi.org/10.3390/cells9040792.
31. Lee, E.S., Lee, J.Y., Kim, G.H., and Jeon, C.J. (2019). Identification of calretinin-expressing retinal ganglion cells projecting to the mouse superior colliculus. Cell Tissue Res. *376*, 153–163. https://doi.org/10.1007/s00441-018-2964-1.
32. Mansour-Robaey, S., Clarke, D.B., Wang, Y.C., Bray, G.M., and Aguayo, A.J. (1994). Effects of ocular injury and administration of brain-derived neurotrophic factor on survival and regrowth of axotomized retinal ganglion cells. Proc. Natl. Acad. Sci. USA *91*, 1632–1636. https://doi.org/10.1073/pnas.91.5.1632.
33. Marchese, A., Giuffrè, C., Cicinelli, M.V., Arrigo, A., Bandello, F., and Battaglia Parodi, M. (2022). The identification of activity of choroidal neovascularization complicating angioid streaks. Eye (Lond) *36*, 1027–1033. https://doi.org/10.1038/s41433-021-01555-5.

34. Álvarez-Aznar, A., Martínez-Corral, I., Daubel, N., Betsholtz, C., Mäkinen, T., and Gaengel, K. (2020). Tamoxifen-independent recombination of reporter genes limits lineage tracing and mosaic analysis using CreERT2 lines. Transgenic Res. *29*, 53–68. https://doi.org/10.1007/s11248-019-00177-8.

35. Huang, W., Xu, Q., Liu, F., Su, J., Xiao, D., Tang, L., Hao, Z.Z., Liu, R., Xiang, K., Bi, Y., et al. (2022). Identification of TPBG-Expressing Amacrine Cells in DAT-tdTomato Mouse. Invest. Ophthalmol. Vis. Sci. *63*, 13. https://doi.org/10.1167/iovs.63.5.13.

36. Zhang, Y., Kao, W.W.Y., Hayashi, Y., Zhang, L., Call, M., Dong, F., Yuan, Y., Zhang, J., Wang, Y.C., Yuka, O., et al. (2017). Generation and Characterization of a Novel Mouse Line, Keratocan-rtTA (KeraRT), for Corneal Stroma and Tendon Research. Invest. Ophthalmol. Vis. Sci. *58*, 4800–4808. https://doi.org/10.1167/iovs.17-22661.

37. Savery, D., Maniou, E., Culshaw, L.H., Greene, N.D.E., Copp, A.J., and Galea, G.L. (2020). Refinement of inducible gene deletion in embryos of pregnant mice. Birth Defects Res. *112*, 196–204. https://doi.org/10.1002/bdr2.1628.

38. Ved, N., Curran, A., Ashcroft, F.M., and Sparrow, D.B. (2019). Tamoxifen administration in pregnant mice can be deleterious to both mother and embryo. Lab. Anim. *53*, 630–633. https://doi.org/10.1177/0023677219856918.

39. Wattez, J.S., Qiao, L., Lee, S., Natale, D.R.C., and Shao, J. (2019). The platelet-derived growth factor receptor alpha promoter-directed expression of cre recombinase in mouse placenta. Dev. Dyn. *248*, 363–374. https://doi.org/10.1002/dvdy.21.

40. Kwon, O.J., Lee, E.S., and Jeon, C.J. (2014). Density and types of calretinin-containing retinal ganglion cells in rabbit. Neuroscience *278*, 343–353. https://doi.org/10.1016/j.neuroscience.2014.08.025.

41. Williams, P.R., Benowitz, L.I., Goldberg, J.L., and He, Z. (2020). Axon Regeneration in the Mammalian Optic Nerve. Annu. Rev. Vis. Sci. *6*, 195–213. https://doi.org/10.1146/annurev-vision-022720-094953.

42. Vidal-Sanz, M., Salinas-Navarro, M., Nadal-Nicolás, F.M., Alarcón-Martínez, L., Valiente-Soriano, F.J., de Imperial, J.M., Avilés-Trigueros, M., Agudo-Barriuso, M., and Villegas-Pérez, M.P. (2012). Understanding glaucomatous damage: anatomical and functional data from ocular hypertensive rodent retinas. Prog. Retin. Eye Res. *31*, 1–27. https://doi.org/10.1016/j.preteyeres.2011.08.001.

43. Boitet, M., Eun, H., Lee, T., Kim, J., and Grailhe, R. (2022). Non-invasive In Vivo Brain Astrogenesis and Astrogliosis Quantification Using a Far-red E2-Crimson Transgenic Reporter Mouse. Mol. Neurobiol. *59*, 6740–6753. https://doi.org/10.1007/s12035-022-02997-y.

44. Joseph, A., Power, D., and Schallek, J. (2021). Imaging the dynamics of individual processes of microglia in the living retina in vivo. Biomed. Opt Express *12*, 6157–6183. https://doi.org/10.1364/BOE.426157.

45. Wahl, D.J., Ng, R., Ju, M.J., Jian, Y., and Sarunic, M.V. (2019). Sensorless adaptive optics multimodal en-face small animal retinal imaging. Biomed. Opt Express *10*, 252–267. https://doi.org/10.1364/BOE.10.000252.

46. Alavi, M.V., Chiang, W.C., Kroeger, H., Yasumura, D., Matthes, M.T., Iwawaki, T., LaVail, M.M., Gould, D.B., and Lin, J.H. (2015). In Vivo Visualization of Endoplasmic Reticulum Stress in the Retina Using the ERAI Reporter Mouse. Invest. Ophthalmol. Vis. Sci. *56*, 6961–6970. https://doi.org/10.1167/iovs.15-16969.

47. Rambout, X., Detiffe, C., Bruyr, J., Mariavelle, E., Cherkaoui, M., Brohée, S., Demoitié, P., Lebrun, M., Soin, R., Lesage, B., et al. (2016). The transcription factor ERG recruits CCR4-NOT to control mRNA decay and mitotic progression. Nat. Struct. Mol. Biol. *23*, 663–672. https://doi.org/10.1038/nsmb.3243.

48. Aguero, T., Zhou, Y., Kloc, M., Chang, P., Houliston, E., and King, M.L. (2016). Hermes (Rbpms) is a Critical Component of RNP Complexes that Sequester Germline RNAs during Oogenesis. J. Dev. Biol. *4*, 2. https://doi.org/10.3390/jdb4010002.

49. Barnhart, M.D., Yang, Y., Nakagaki-Silva, E.E., Hammond, T.H., Pizzinga, M., Gooding, C., Stott, K., and Smith, C.W.J. (2022). Phosphorylation of the smooth muscle master splicing regulator RBPMS regulates its splicing activity. Nucleic Acids Res. *50*, 11895–11915. https://doi.org/10.1093/nar/gkac1048.

50. Hörnberg, H., Wollerton-van Horck, F., Maurus, D., Zwart, M., Svoboda, H., Harris, W.A., and Holt, C.E. (2013). RNA-binding protein Hermes/RBPMS inversely affects synapse density and axon arbor formation in retinal ganglion cells in vivo. J. Neurosci. *33*, 10384–10395. https://doi.org/10.1523/JNEUROSCI.5858-12.2013.

51. Hörnberg, H., Cioni, J.M., Harris, W.A., and Holt, C.E. (2016). Hermes Regulates Axon Sorting in the Optic Tract by Post-Trancriptional Regulation of Neuropilin1. J. Neurosci. *36*, 12697–12706. https://doi.org/10.1523/JNEUROSCI.2400-16.2016.

52. Madisen, L., Zwingman, T.A., Sunkin, S.M., Oh, S.W., Zariwala, H.A., Gu, H., Ng, L.L., Palmiter, R.D., Hawrylycz, M.J., Jones, A.R., et al. (2010). A robust and high-throughput Cre reporting and characterization system for the whole mouse brain. Nat. Neurosci. *13*, 133–140. https://doi.org/10.1038/nn.2467.

STAR★METHODS

KEY RESOURCES TABLE

REAGENT or RESOURCE	SOURCE	IDENTIFIER
Antibodies		
Rabbit polyclonal anti-RBPMS	Thermo Fisher Scientific	Cat# PA5-31231; RRID: AB_2548705
Mouse monoclonal anti- beta III Tubulin (Tuj-1)	Abcam	Cat# ab78078; RRID: AB_3064854
Rabbit polyclonal anti-Calretinin	Abcam	Cat# ab702; RRID: AB_305702
Sheep polyclonal anti-Chx10 (VSX2)	Sigma-Aldrich	Cat# AB9016; RRID: AB_3064860
Rabbit polyclonal anti-Recoverin	Sigma-Aldrich	Cat# AB5585; RRID: AB_3064861
Rabbit polyclonal anti-alpha smooth muscle Actin	Abcam	Cat# ab5694; RRID: AB_2223021
Goat polyclonal anti-tdTomato	arigo	Cat# ARG55724; RRID: AB_3064862
Rabbit monoclonal anti-alpha Actinin	Abcam	Cat# ab68194; RRID: AB_3064857
Rabbit monoclonal anti-Cardiac Troponin T (cTnT)	Abcam	Cat# ab209813; RRID: AB_2938619
Rabbit monoclonal anti-PDGFR alpha+PDGFR beta	Abcam	Cat# ab32570; RRID: AB_777165
Rabbit monoclonal anti-GAPDH	Cell Signaling Technology	Cat#2118S; RRID: AB_3064901
Alexa Fluor 488 Donkey Anti-Mouse IgG (H + L)	Thermo Fisher Scientific	Cat# A-21202; RRID: AB_141607
Alexa Fluor 555 Donkey Anti-Mouse IgG (H + L)	Thermo Fisher Scientific	Cat# A-31570; RRID: AB_2536180
Alexa Fluor 488 Donkey Anti-Rabbit IgG (H + L)	Thermo Fisher Scientific	Cat# A-21206; RRID: AB_2535792
Alexa Fluor 555 Donkey Anti-Rabbit IgG (H + L)	Thermo Fisher Scientific	Cat# A-31572; RRID: AB_162543
Alexa Fluor 647 Donkey Anti-sheep IgG (H + L)	Abcam	Cat# ab150179; RRID: AB_2884038
Alexa Fluor 488 Donkey Anti-Goat IgG (H + L)	Thermo Fisher Scientific	Cat# A-11055; RRID: AB_2534102
Chemicals, peptides, and recombinant proteins		
Donkey serum	Solarbio	Cat# SL050
MEM Non-Essential Amino Acids	Gibco	Cat# 11140050
RIPA lysis buffer	Beyotime	Cat# P0013B
Tamoxifen	Sigma-Aldrich	Cat# T5648
Trizol Reagent	Thermo Fisher Scientific	Cat# 15596026
Protease inhibitor mixture	Beyotime	Cat# P1045-2
DNA ladder	Solarbio	Cat# M1100
SDS-PAGE Sample Loading Buffer	Beyotime	Cat# P0015
Antifade Mounting Medium	Beyotime	Cat# P0126
4% Paraformaldehyde Fix Solution	Beyotime	Cat# P0099
Critical commercial assays		
BCA quantitative kit	Beyotime	Cat# P0012S
Chemiluminescent HRP Substrate	Millipore	Cat# WBKLS0500
2 × Taq Master Mix (Dye Plus)	Vazyme	Cat# P112-03
TIANamp genomic DNA kit	TIANGEN	Cat# DP304
ChamQ SYBR Color qPCR Master Mix	Vazyme	Cat# Q431-02
Experimental models: Organisms/strains		
Mouse: C57BL/6J	The Jackson Laboratory	RRID: IMSR_JAX:000664
Mouse: B6; 129S6-Gt (ROSA)26Sor$^{tm9(CAG-tdTomato)Hze/J}$	The Jackson Laboratory	RRID: IMSR_JAX:007905
Mouse: B6/JGpt-Rbpms$^{em1Cin\ (CreERT2-P2A)/Gpt}$	This paper	N/A
Mouse: RBPMS$^{CreERT2-tdTomato}$	This paper	N/A

(*Continued on next page*)

Continued

REAGENT or RESOURCE	SOURCE	IDENTIFIER
Oligonucleotides		
RBPMS gRNAs	AGGACCGGGAAGATGAACGG	CGAAGGACCGGGAAGATGAA
See Table S1 for primer sequences	This paper	N/A
Recombinant DNA		
Plasmid: pMD-18T	This paper	N/A
Software and algorithms		
Fiji/ImageJ	National Institutes of Health (NIH)	https://fiji.sc/
FlowJo™ v10.8	Becton, Dickinson and Company (BD)	https://www.flowjo.com
Photoshop	Adobe	N/A
TissueFAXS Viewer 7.1	TissueGnostics	https://tissuegnostics.com/products/scanning-and-viewing-software/tissuefaxs-viewer

RESOURCE AVAILABILITY

Lead contact

Further information and requests for resources and reagents should be directed to and will be fulfilled by the lead contact, Yingfeng Zheng (zhyfeng@mail.sysu.edu.cn).

Materials availability

Murine models generated in this study, namely RBPMS $^{CreERT2-tdTomato}$ mice. Materials generated in this study are available from the lead contact's laboratory upon request.

Data and code availability

- All data reported in this paper will be shared by the lead contact upon request (zhyfeng@mail.sysu.edu.cn).
- This paper does not report original code.
- Any additional information required to reanalyze the data reported in this paper is available from the lead contact upon request.

EXPERIMENTAL MODEL AND STUDY PARTICIPANT DETAILS

Generation of mouse line

All mice were conducted with the approval of the animal ethics committees of Zhongshan Ophthalmic Center and SUN YAT-SEN University, and in compliance with the ARVO Statement for the Use of Animals in Ophthalmic and Vision Research. The animals were kept under a 12-h light/dark cycle alternating schedule.

The RBPMS knock-in protocol was designed based on RBPMS-CCDS40318 (Gene ID:19663, NCBI), which have seven exons within encoding 1039 bp transcripts and 220 amino acids. The CRISPR/Cas9 method employed three key components: gRNAs (5′-3′: AGGACCGG GAAGATGAACGG and CGAAGGACCGGGAAGATGAA), the Cas9 protein to create double-stranded DNA breaks in the genome, and the ssDNA donor vector (pMD-18T) as a template for repairing the breaks. The three ribonucleoprotein complexes (gRNA, Cas9, and donor vector) were microinjected into mouse zygotes. Living gene-edited zygotes were selected and implanted into pseudo-pregnant mice, resulting in the first generation (F0) of offspring. F0 founders with confirmed genotypes were then bred with wild-type (WT) mice to generate the F1 animal generation, producing RBPMSCreERT2 mice. RBPMSCreERT2 mice were crossed with Ai9 tdTomato reporter mice (B6; 129S6-Gt (ROSA)26Sor$^{tm9(CAG-tdTomato)Hze/J}$),[52] resulting in the generation of RBPMSCreERT2-tdTomato mice. Male and female RBPMS$^{KI/+}$ mice, except when indicated, were used in the study.

Optic nerve crush (ONC)

The 4–8 weeks adult RBPMS$^{CreERT2-tdTomato}$ mice underwent an optic nerve crush procedure after being induced with tamoxifen. The mice were first anesthetized using isoflurane, and then the surrounding conjunctiva was incised to expose the optic nerve. The optic nerve was crushed 1 mm away from the optic disc using reverse-action forceps for 10 s. The ONC mice model were euthanized and enucleated the eyeball for frozen sections and retinal wholemount analysis.

Laser-induced choroidal neovascularization (CNV) and OCT-angiography

The 4–8 weeks adult RBPMS$^{CreERT2-tdTomato}$ mice mice were anesthetized with isoflurane and their pupils were dilated three times using compound tropicamide eye drops. Laser burns were then induced under a red fluorescence filter using an ophthalmic therapy laser (Zeiss,

Germany) with a sliding glass contact lens. Four laser burns (532 nm wavelength, 200 mW output energy, 50 ms duration and 50 μm hole size) were applied to each eye, surrounding the optic disc and intervascular areas. Images were taken at days 3, 7, and 12 following the laser-induced burns, based on the natural tdTomato fluorescence signal. Optical coherence tomography (OCT, Heidelberg Engineering, Germany) was used to image the fundus and to perform tdTomato-based fluorescence angiography.

METHOD DETAILS

Genotyping verification by PCR and DNA sequence

Genomic DNA was extracted from the tails of 3-week-old mice, and PCR and DNA sequencing were performed for genotype identification. The tail DNA extraction and amplification were conducted using the TIANamp genomic DNA kit (TIANGEN, China) and Vazyme-P222 rapid taq master mix (Vazyme, China) according to the manufacturer's specifications. In brief, a 2-3 mm piece of the mouse tail was placed in 200ul extraction buffer and incubated at 55°C for 12 h. Double the volume of ethanol was then added and the mixture was centrifuged. The DNA precipitation was dissolved in deionized water. For the PCR procedure, 20 ng of DNA extract was added to 12.5μL of 2×taq mix and 10 pmol/μL primers. PCR amplification conditions for RBPMS Cre/WT alleles were 95°C for 30 s for 35 cycles, ending at 72°C for 5 min (ABI, America). The amplified products were separated on a 1–3% agarose gel and photographed. The gel-purified amplicons were then subjected to sequencing using PCR primers and/or internal primers. The primers are listed in Table S1.

Tamoxifen induction

Tamoxifen (Sigma) was dissolved in corn oil at a concentration of 20 mg/ml by shaking overnight in the absence of light. Adult mice were administered a dose of approximately 75 mg/kg body weight via intraperitoneal injection once every 24 h for five consecutive days. There was a seven-day waiting period between the final injection and histological analysis. Pregnant mice were exposed to four consecutive doses of 75 mg/kg body weight tamoxifen starting at E10.5 and were sampled four days after the final exposure.

Tissue preparation and immunohistochemistry fluorescence staining

For preparing cultured cells for analysis, cells were fixed with 4% paraformaldehyde (PFA) (Beyotime) for 10 min. The cells were then washed twice with 0.01 M PBS. For organoid frozen sections, the organoids were collected, washed with 0.01 M PBS, and fixed with 4% PFA for 30 min at room temperature. The fixed organoids were then subjected to a sucrose gradient dehydration process, with concentrations increasing from 6.25% to 12.5%–25%. In the case of frozen tissue sections, eyeballs were collected, washed with 0.01 M PBS, fixed with 4% PFA overnight at 4°C, and dehydrated with 30% sucrose overnight at 4°C. Both the organoids and tissues were then sliced into 8–10 μm sections using a Leica microtome (Leica CM 1950).

Cells or sections were incubated in a blocking solution containing 10% donkey serum (Solarbio) only or 10% donkey serum with 0.25% Triton X-100 for 1 h at room temperature. The primary antibodies were then added at an appropriate dilution in PBS and incubated overnight at 4°C. Following the primary antibody incubation, the cells or sections were washed three times with 0.01 M PBS and incubated with secondary antibodies for 1 h at room temperature. Nuclear counterstaining was performed using DAPI (40,6-diamidino-2-phenylindole) (Sigma-Aldrich). Images were captured using a Zeiss fluorescence microscope (Axio Observer 7) and whole tissue images were obtained using the Tissue fax confocal imaging system (Zeiss, Germany). Information on the antibodies used can be found in Table S2.

The primary heart cells culture and tdTomato-based FACS sorting

The biopsies of heart were dissected and mechanically cut into 2-3 mm pieces in a basic culture medium containing 10% antibiotics (Gibco). The primary tissue explants were then cultured in six well plates with added medium containing 10% FBS (Gibco) and 1% NEAA (Gibco). The monolayer cells were observed to crawl out from the adherent explants, while others remained suspended and were isolated for culture in low-attachment dishes, forming organoids. The primary heart cells were digested into single cells for FACS sorting basing tdTomato fluorescence signals, the collected tdTomato positive cells were culture on six well plates.

qRT-PCR

The tissues and cells were collected and RNA extraction was performed using TRIzol Reagent (Thermo Fisher) according to the manufacturer's instructions. One microgram of RNA was then reverse transcribed using random primers. Quantitative Real-Time PCR (qRT-PCR) was conducted using an SYBR Green reaction mixture (Vazyme) on a Quant Studio 7 Flex system (Applied Biosystems). The levels of target gene expression were determined using the comparative cycle threshold (Ct) method and normalized to GAPDH. The fold changes were calculated using the formula $2^{-\Delta\Delta Ct}$. The primer sequences can be found in Table S1.

Western blot

The tissues were cut into pieces and added the 200μL RIPA lysis buffer (Beyotime) per 25 mg tissue sample, and supplemented with 1x protease inhibitor mixture (Beyotime). The lysates were centrifuged at 13000 RPM for 15 min and collected the supernatant. The protein concentration was examined by BCA quantitative kit. Immunoblotting was performed by standard protocols with 5 μg protein lysate per well. Primary antibodies used were RBPMS (1:1000, Invitrogen) and GAPDH (1:1000, CST) incubation for overnight at 4°C, and HRP-linked second antibody

was incubation for 2 h at room temperature, and the blots were developed using Western Chemiluminescent HRP substrate reagent (Millipore).

QUANTIFICATION AND STATISTICAL ANALYSIS

Data are presented as the mean ± standard error of the mean (SEM). For qRT-PCR assay, data were collected from at least three technical replicates, and ΔΔCt method was used for computing the relative expression level. For Western blot assay, the gray values of protein bands were measured by ImageJ and the protein expression were calibrated by internal reference GAPDH.